Nanoscale

PAPER

Cite this: *Nanoscale*, 2015, **7**, 12868

Insights into the effects of metal nanostructuring and oxidation on the work function and charge transfer of metal/graphene hybrids

M. M. Giangregorio,*[a] W. Jiao,[b] G. V. Bianco,[a] P. Capezzuto,[a] A. S. Brown,[b] G. Bruno[a] and M. Losurdo*[a,b]

Received 22nd April 2015,
Accepted 23rd June 2015

DOI: 10.1039/c5nr02610e

www.rsc.org/nanoscale

Graphene/metal heterojunctions are ubiquitous in graphene-based devices and, therefore, have attracted increasing interest of researchers. Indeed, the literature on the field reports apparently contradictory results about the effect of a metal on graphene doping. Here, we elucidate the effect of metal nanostructuring and oxidation on the metal work function (WF) and, consequently, on the charge transfer and doping of graphene/metal hybrids. We show that nanostructuring and oxidation of metals provide a valid support to frame WF and doping variation in metal/graphene hybrids. Chemical vapour-deposited monolayer graphene has been transferred onto a variety of metal surfaces, including d-metals, such as Ag, Au, and Cu, and sp-metals, such as Al and Ga, configured as thin films or nanoparticle (NP) ensembles of various average sizes. The metal-induced charge transfer and the doping of graphene have been investigated using Kelvin probe force microscopy (KPFM), and corroborated by Raman spectroscopy and plasmonic ellipsometric spectroscopy. We show that when the appropriate WF of the metal is considered, without any assumption, taking into account WF variations by nanostructure and/or oxidation, a linear relationship between the metal WF and the doping of graphene is found. Specifically, for all metals, nanostructuring lowers the metal WF. In addition, using gold as an example, a critical metal nanoparticle size is found at which the direction of charge transfer, and consequently graphene doping, is inverted.

1. Introduction

Understanding the metal–graphene interaction based on charge transfer from/to a metal to/from a graphene layer is both fundamentally and technologically relevant for a number of reasons:

(i) metal–graphene interactions regulate the chemical vapor deposition (CVD) of graphene on transition metals;[1]

(ii) a graphene–metal heterojunction is an essential element in graphene-based devices, such as gas sensors, supercapacitors, printed electronics and photodetectors;

(iii) in graphene electronics, the metal–graphene contact resistance limits the on-current of graphene field-effect transistors (FETs), while in graphene optoelectronics a strong band bending in the vicinity of the metal–graphene junction can lead to efficient photocurrent;[2]

(iv) metal nanoparticles (NPs), mainly gold (Au) and silver (Ag), have been used to both tune the visible spectrum and enhance absorption of graphene through localized surface plasmon resonance (LSPR)[3] for building new electrocatalysts for fuel cells;[4]

(v) graphene–metal (Au, Ag, Pt and Pd) NPs have been synthesized using graphene oxide sheets as a precursor in solution approaches[5,6] to obtain nanocomposites for sensing and catalysis;[7]

(vi) ultrathin metal layers and nanoparticles have been investigated both theoretically[8–11] and experimentally[12–19] to modulate the work function (WF) of graphene by metal doping.

Therefore, the WF of both graphene and the metal comprising a hybrid functional platform is one of the most important properties affected by the charge at the metal/graphene interface.

To date, graphene has been coupled to a broad range of metals that are primarily grouped into two categories, *i.e.*, physisorbed metals such as Cu, Au, Ag, Al, and Pt, which do not significantly affect the π-band dispersion of graphene, but can affect its doping by charge transfer from/to these metals, and chemisorbed metals such as Ni, Co, Cr, Pd, and Ti that destroy

[a]*CNR-NANOTEC, Istituto di Nanotecnologia and IMIP-Institute of Inorganic Methodologies and of Plasmas, via Orabona, 4, 70126 Bari, Italy. E-mail: michelaria.giangregorio@imip.cnr.it, maria.losurdo@cnr.it*
[b]*Electrical and Computer Engineering Department, Duke University, Durham 27708, NC, USA*

the graphene π-band dispersion around the Dirac point due to strong hybridization between metal-d and carbon-π orbitals.[20,21]

Focusing solely on the former category with relatively weak metal/graphene interfaces, formed from metals (Cu, Ag, Au, Al, Ga) with adsorption energies around 0.03–0.05 eV per carbon atom and with equilibrium interfacial distances >3 Å,[20] we can further subcategorize them into d-metals (Cu, Ag, Au) and sp-metals (Al, Ga). The charge transfer at these interfaces is differentially affected by the interaction of the metal s- or d-electrons with the π-electrons of graphene.

While being an area of intense research interest, results are often contradictory; hence, further research is needed to develop a deeper understanding of interfacial charge transfer. As an example, it has been reported that Ag deposition induces n-type doping, whereas Au deposition induces p-type doping of exfoliated graphene.[22] On the other hand, Ruoff's work[15] showed that Au could lead to either p-type or n-type doping of CVD graphene, depending on the nanostructuring of the Au. Various noble metals, *e.g.* Ag, Au, Pt and Pd, and nanoparticles (NPs) were also investigated by Subrahmanyam *et al.*,[23] who examined their interaction with graphene using Raman spectroscopy and first-principles calculations, reporting electron transfer from graphene to metal nanoparticles for Pd, Ag, Pt, *i.e.*, p-type doping of graphene by Ag, and from metal nanoparticles to graphene for Au, *i.e.*, n-doping of graphene by Au. Those results seem to contradict those of Novoselov,[22] who reported n-doping of graphene by Ag and p-doping of graphene by Au. Indeed, in the study by Subrahmanyam *et al.*[23] graphene samples were prepared by thermal exfoliation of graphite oxide (GO) followed by reduction in hydrogen, while metal NPs were obtained from solution salts, whereas Novoselov[22] investigated exfoliated graphene on evaporated Ag and Au NPs. Those contradictions point out the importance of the specific graphene synthesis methodologies (exfoliated, chemical vapor deposited (CVD), reduced-GO with various functional groups), the thickness of the graphene, and the synthesis of the metal layer (*e.g.*, sputtered, evaporated or from salts in solutions that can introduce additional surfactants interacting with graphene). All of these factors influence the work functions of the metal and graphene. In order to understand the metal doping effect, the advantages and limits of the various approaches exploited to determine the WF of graphene have to be taken into account. As an example, the exploited approaches include current–voltage[24,25] and capacitance–voltage measurements,[13] which, however, refer to graphene under the metal, and photoelectron spectroscopy (PS)[17,26] that can be applied to investigate both graphene-on-metal and metal-on-graphene configurations, and which are, however, affected by artefacts induced by the UV exposure typical of UPS measurements.[27]

To give an example of the complexity of the graphene WF determination, Fig. 1 summarizes reported theoretical and experimental data of the Fermi level shift, ΔE_F, of various metal-doped CVD graphene. It is seen that the spread in data is quite large: as an example of the Au/G heterostructure a variation of the value of WF_{Au} from 4.7 eV to 5.6 eV can result in a ΔE_F for graphene ranging from approximately 0.08 eV to 0.3 eV. Similarly, a large spread of data is seen for the Cu/G couple. Some discrepancies between theoretical and experimental data have been explained by Giovannetti *et al.*[8] with a phenomenological model in which Pauli's repulsive interaction and electron transfer are assigned as two main factors influencing interfacial doping. Pauli's repulsive interaction and the metal–graphene distance were introduced by Giovanetti[8] to explain why metals like Au (WF of 5.54 eV), Ni (WF of 5.47 eV) and Co (WF of 5.44 eV) with similar WF values were reported to give p-type (Au) and n-type (Ni, Co) doping of graphene, respectively.

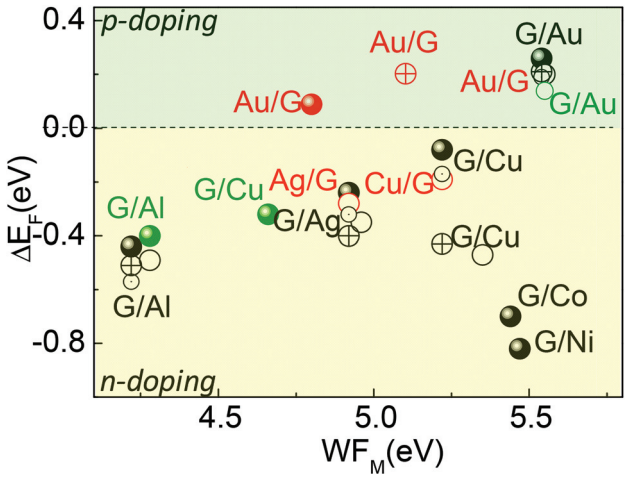

Fig. 1 Theoretical (black circles: ● [8], ○ [9], ⊙ [10] and ⊕ [11]) and experimental (red and green circles: O [12], ● [13], ⊕ [15], ● [16] and O [17]) literature data of the Fermi level shifts, ΔE_F, of metal-doped CVD graphene as a function of the metal work function, WF_M. M/G refers to metal-on-graphene, while G/M refers to graphene-on-metal.

Here we take and present a different perspective, answering the question: can the apparent discrepancies about the WF and the metal doping effect of graphene be framed by a rationale that considers chemical and structural effects on the metal WF (which cannot be assumed stiff at the theoretical value)?

Specifically, we show that the metal-based doping of graphene is critically dependent on the work function of the metal and the observed variability is a direct result of the process-, oxidation- and structure-dependent work function of the metal.

In order to support this rationale, we study graphene on metal thin films and nanoparticles (NPs) from two main groups: the sp-metals, *i.e.*, Al and Ga, and the noble d-metals, *i.e.*, Ag, Au and Cu. This choice is because sp- and d-metals have different interactions with graphene. Specifically, for Al and Ga sp-metals, the interaction with graphene is predominantly ionic, without strong hybridization between the pz orbitals of graphene and the metal valence electrons, so that the electron transfer is only driven by the difference between the work functions of the metal and graphene. In contrast, Cu, Ag and Au d-metals have lower equilibrium separation compared

to sp-metals with, consequently, a significant influence on the charge transfer from/to graphene.[8]

A multidiagnostic corroborating approach is exploited to investigate the charge transfer between graphene and the metal. Specifically, measurements of the change of WF have been performed exploiting Kelvin probe force microscopy (KPFM). The use of this technique was recently shown to be valid for graphene through testing against density functional theory (DFT) calculations by Ziegler *et al.*[28]

Key points underlying the present work are:

(i) we do not make any assumption about the WFs of either the CVD graphene or metals. The measured value is used for our analysis. This is an important point, since the work function of the metal is known to depend on its structure, thin film or nanostructured, crystalline orientation,[29] and oxidation state.[30–33] The scatter in the ΔE_F data for Au/graphene is a result of the use of assumed Au WF values. In Fig. 1, the theoretical work assumed a WF of 5.54 eV for the atomically clean Au (111) surface,[8] whereas the experimental measurements of the WF of evaporated Au, subsequently exposed to air or contaminated with organic films, yielded values as low as 4.5 eV,[31,32] consequently inverting the charge transfer from/to graphene.

(ii) We analyse the dependence of the graphene ΔE_F and of the metal WF on metal nanostructuring and average nanoparticle size in the NP ensemble. The metal WF and charge transfer at the interface with graphene depend upon the metal structure.[34,35]

(iii) We also consider the effect of metal oxidation on its WF and, consequently, on charge transfer. Silver (Ag) and copper (Cu) can be taken as an example of the effect of oxidation on the WF. Specifically, (110), (100) and (111) clean Ag surfaces have WF values of 4.14, 4.22 and 4.46 eV, respectively, which make possible n-doping of graphene. Indeed, the Ag WF increases to 4.65 eV, 4.52 eV, and 4.75 eV with oxidation and polycrystallinity,[36,37] possibly activating p-doping of graphene. Conversely, the WF of clean Cu of 5.22 eV[8] can decrease by oxidation from 5.2–5.6 eV for CuO to 4.8 eV for Cu_2O, and to 4.35 eV by polycrystallinity,[38] possibly switching from p-doping to n-doping of graphene.

(iv) We also investigate the importance of the graphene/metal hybrid configuration. Most of the existing reported experimental work is for the metal-on-graphene configuration.[12–15,19,39] Indeed, metal deposition on the graphene lattice, *e.g.*, by electron beam nanofabrication, can induce disorder in the graphene lattice,[40] while colloidal metal nanoparticles can leave residual capping agents; both factors affect the WF. Therefore, we directly characterize graphene transferred onto metals. Furthermore, the Pauli repulsive interaction also depends on the graphene–metal separation, as theoretically predicted by Giovannetti *et al.*[8] and the graphene–metal separation changes depending on the metal–graphene configuration.

(v) Finally, KPFM-derived charge transfer is corroborated by Raman spectroscopy and spectroscopic ellipsometry,[41] the latter also revealing the impact of the metal/graphene charge transfer on the plasma frequency, ω_p, of the metal in contact with graphene, and on the localized surface plasmon resonance (LSPR) of the metal/graphene nanohybrids.[18]

2. Experimental

Graphene growth and transfer

Graphene was grown on Cu foils by chemical vapor deposition (CVD) from mixtures of $CH_4 : H_2$ = 100 : 0–50 sccm gases at a temperature of 1000 °C and at a total pressure of 1 Torr in a barrel CVD reactor. The samples were then cooled at a rate of ~2 °C min^{-1} in 1 Torr of H_2.[42–44]

After growth, graphene was transferred onto different metal samples by the thermal tape method. This choice was to avoid any interlayer of water/solvent trapped at the metal/graphene interface that could alter the charge transfer and, hence, the WF measurements. Furthermore, by topography measurements run before and after the thermal release at 120 °C on an area of the sample exposing the metal film or NPs, we verified that the thermal exposure (a few seconds) did not alter the morphology of the metal.

Metal deposition

Nanoparticles and films of Au, Ag, and Cu were evaporated on Corning glass substrates, while Ga NPs and Al NPs of controlled size were obtained by molecular beam epitaxy (MBE) in a Veeco GEN II system under ultrahigh vacuum conditions at room temperature.[18] The metal evaporation time was used as a parameter to tune the NP size or film thickness.

Characterization

Raman spectroscopy. Raman spectra were collected using a LabRAM HR Horiba-Jobin Yvon spectrometer using the 532 nm with a laser power of 0.1 mW to avoid any damage to the graphene and a 100× objective lens with a Numerical Aperture (NA) = 0.95 laser. Raman spectra of graphene on Cu were acquired with a blue laser (473 nm) to suppress the Cu photoluminescence background. The Raman band of a silicon wafer at 520 cm^{-1} was used to calibrate the spectrometer, and the accuracy of the spectral measurement was estimated to be better than 1 cm^{-1}.

X-ray photoelectron spectroscopy. XPS analysis was run to check metal oxidation using a Kratos system with a monochromatized Al Kα source. High resolution spectra of the Al 2p, Ga 3d, Cu 2p, Ag 3d, C 1s, and O 1s photoelectron core levels were acquired at take-off angles of 90°. The peaks were resolved with Gaussian and Lorentzian fitting with the following boundary conditions imposed: (i) the FWHM of each chemical component was fixed, (ii) the adventitious carbon was fixed at 285 eV. The spectrometer was calibrated by setting the binding energy of the Au 4f7/2 peak to 84.0 eV. For graphene on glass the Csp^2 component in the C 1s peak was found at 284.5 eV.

Spectroscopic ellipsometry. SE was used to detect the effect of the charge transfer on the localized surface plasmon resonance (LSPR) of metal NPs/graphene hybrids. SE measured the

ratio, ρ, of the Fresnel reflection coefficients of the two components of light, r_p and r_s, polarized, respectively, parallel and perpendicular to the plane of incidence, according to the equation[44]

$$\rho = r_p/r_s = \tan \Psi \exp(i\Delta) \quad (1)$$

where Ψ and Δ are the ellipsometric angles, Ψ being the amplitude ratio ($\tan \Psi = |r_p|/|r_s|$) and Δ the phase difference ($\Delta = \delta_p - \delta_s$) between the p and s components.

The pseudodielectric function, $\langle\varepsilon\rangle$, was derived from the ρ parameter using the following equation:

$$\langle\varepsilon\rangle = \langle\varepsilon_1\rangle + i\langle\varepsilon_2\rangle = \sin^2 \Phi_0[1 + \tan^2 \Phi_0(1-\rho)^2/(1+\rho)^2] \quad (2)$$

at an angle of incidence Φ_0 of 70°. Spectra of the pseudodielectric function, $\langle\varepsilon\rangle = \langle\varepsilon_1\rangle + i\langle\varepsilon_2\rangle$, of the various metal-graphene samples were acquired in the photon energy range 191–826 nm using a phase modulated spectroscopic ellipsometer (UVISEL—Jobin Yvon).

Kelvin probe force microscopy. The work functions of the metal films, metal nanoparticles, undoped graphene and metal-doped graphene were measured by Kelvin probe electrical force microscopy (KPFM) using the Autoprobe CP (Thermomicroscope) through the measurement of the local variation of the surface potential (SP). The sample topography and SP were recorded in a single-pass mode[45–48] using gold-coated Si tips (their frequency was ~80 Hz) in non-contact mode. The oscillating potential, V_{ac}, applied to the tip was 5 V at a frequency ω of 13 kHz. The samples were electrically connected to the ground of the microscope (the sample stage).

All measurements were collected in air at room temperature. Prior to the imaging, all samples are cleaned and measured soon after the deposition in order to improve the reproducibility and accuracy of the SP measurements that are affected by the surface of the sample (contaminations, uniformity or charging).[49] The ability to obtain quantified, comparable and accurate results by KPFM, even in air, was demonstrated and discussed in detail by Panchal *et al.*[50]

The WF was calibrated against the WF of the gold contact, which was found to be, under ambient conditions, 4.7–4.8 eV,[51] as also corroborated by XPS measurements. The WF of our CVD graphene was found to be 4.53 ± 0.05 eV, consistent with data in the literature with WF values ranging from 4.48 to 4.60 eV.[8,52,53]

3. Results and discussion

Fig. 2 illustrates our use of KPFM to determine the WF of both the investigated metals and the CVD graphene on glass also metal-doped. We transferred graphene on half of the metal film/NP samples, and we scanned the sample from the graphene-on-metal to the graphene (as highlighted by red lines in Fig. 2). A typical SP map, 60 μm × 60 μm, is also shown in Fig. 2. ΔSP, *i.e.* the difference between the SP of the graphene-on-metal, SP_{G-M}, and the SP of the as-transferred graphene on glass, SP_G, which quantifies the shift in the Fermi level of graphene induced by the metal, ΔE_F, was determined using

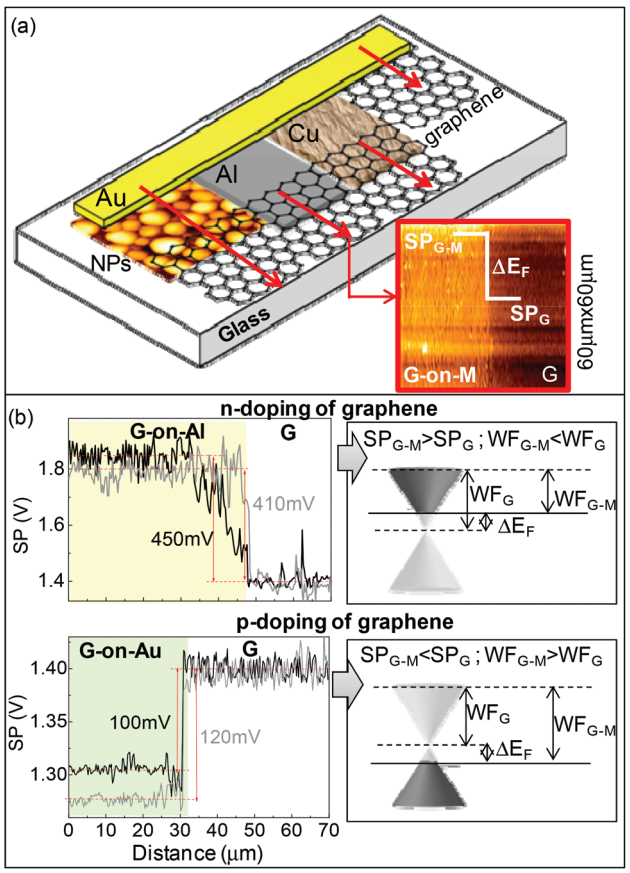

Fig. 2 (a) Scheme of our KPFM approach to measure both the WFs of the investigated metals, of the CVD graphene on glass and the WFs of the metal-doped graphene. A typical SP map, 60 μm × 60 μm, is also shown. (b) Representative SP profiles for graphene-on-Au and graphene-on-Al against the same graphene on glass. For each case in (b), two representative profiles (gray and black lines) are reported to show the reproducibility of the measurements.

$$\Delta SP = SP_{G-M} - SP_G = \Delta E_F$$
$$\Delta E_F = WF_{tip} - WF_{G-M} - WF_{tip} + WF_G = WF_G - WF_{G-M} \quad (3)$$

where WF_{tip} is the tip work function, WF_G is the CVD graphene work function on glass and WF_{G-M} is the work function of metal doped graphene.

Fig. 2 also shows representative SP profiles obtained for graphene-on-Au and graphene-on-Al against the same graphene on glass. Specifically, if the SP of the graphene-on-metal is higher than the SP of the graphene, *i.e.*, $SP_{G-M} > SP_G$, the WF of the graphene-on-metal is lower than that of the graphene, $WF_{G-M} < WF_G$, and hence the metal n-type dopes graphene.

If the SP of the graphene-on-metal is lower than that of graphene on glass, $SP_{G-M} < SP_G$, the WF of the graphene-on-metal is higher than that of the graphene, $WF_{G-M} > WF_G$, and hence the metal p-type dopes graphene.

Fig. 3 shows examples of AFM morphologies of graphene transferred onto nanoparticle samples. The large scale AFM image shows that some ripples developed during the transfer with thermal release tape, and the initial large-area graphene breaks in some points uncovering the NPs underneath. The cross-section profiles for graphene on NPs indicate a gap between graphene and most of the NPs of 0.5–1 nm. This gap is because of the broad size and random distribution of the NPs with the graphene lying and touching the top curvature of the NP and not conformally surrounding each NP. This also explains why for larger Al NPs, the graphene on Al NPs smoothens the profile. Referring to the dependence of the Fermi level shift on the graphene–metal distance published by Giovanetti *et al.*,[8] we are certainly in a distance regime above the equilibrium distance, where for Au a p-type doping should be expected, while for Al, an n-type doping should be expected independently of the distance.

For graphene on Cu in Fig. 4, color contrast in Raman micrographs highlighted regions that the Raman (see spectra in Fig. 4) and XPS (see Fig. 6) analyses confirmed to be due to local oxidation of Cu grains (dark regions – oxidized, light regions – unoxidized). Specifically, the Raman peaks observed in Fig. 4 in the region 190–1000 cm^{-1} are due to Cu_2O and CuO.[54–56] Furthermore, AFM measurements, also shown in Fig. 4, reveal different morphology and adhesion of graphene on oxidized and non-oxidized Cu. Specifically, there are distinct steps on the whole surface of graphene/clean Cu, while no indications of copper steps but the presence of pits and defects have been observed for graphene on oxidized copper grains, consistent with what was reported by Qi *et al.*[54]

Consequently, when measuring the WF, different regions corresponding to graphene/clean Cu and graphene/oxidized Cu have been measured and analyzed as shown in Fig. 4 and reported in Table 1.

Table 1 summarizes the WF measured for the various investigated metals, the shift of the Fermi level, ΔE_F, of the gra-

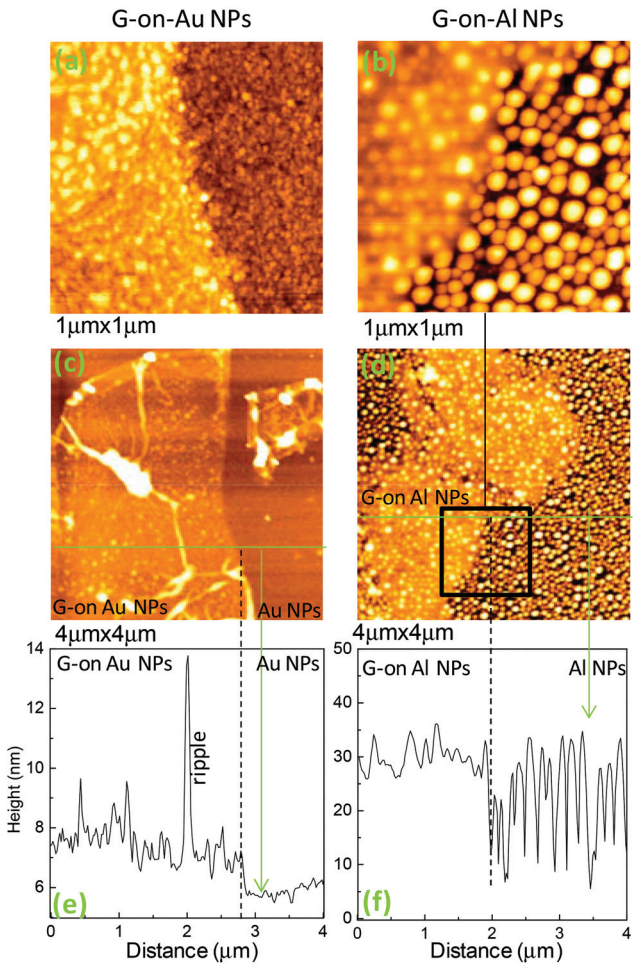

Fig. 3 AFM images of graphene on (a, c) approximately 30 nm Au NPs and on (b, d) average 70 nm Al NPs. The green-lines in (c) and (d) indicate where the cross-section profiles shown in (e) and (f) respectively for graphene-on-Au NPs and for graphene-on-Al NPs have been taken.

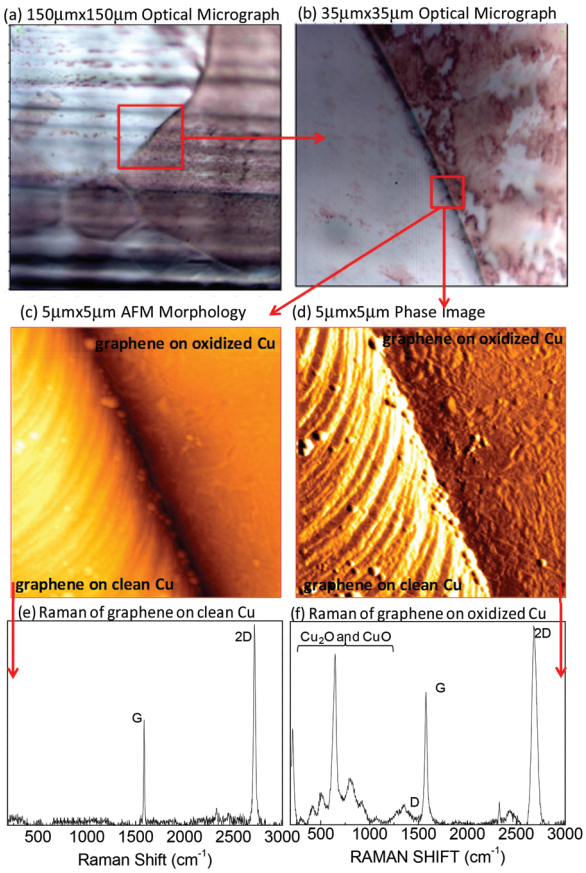

Fig. 4 Optical micrographs of (a) 150 μm × 150 μm and (b) 35 μm × 35 μm graphene on polycrystalline Cu with oxidized areas (brown dark regions) identified by the different color contrast. In (a) and (b) the red-square is just to indicate that the magnified optical micrograph and AFM images have been acquired at the borderline between regions with a clear color contrast. AFM images of (c) topography and (d) phase contrast for graphene at the borderline between clean (left-side of the image) and oxidized (right-side of the image) Cu regions. Raman spectra of (e) clean copper (light gray regions) and of (f) oxidized copper (taken in the brown dark region) taken with the blue laser (473 nm) to suppress the Cu photoluminescence background.

Table 1 Measured values by KPFM of the shift of the Fermi level, ΔE_F, of the graphene due to the doping by the various metals and the corresponding WF of the metal-doped graphene, WF_{G-M} and of metals, WF_M. Theoretical values of the WF of metals from Giovannetti *et al.*[8]

	Metal	ΔE_F (mV)	WF_{G-M} (eV)	WF_M (eV)	WF_M (eV)[8]
	CVD graphene			4.53 ± 0.05	4.6
d-Metals	Poly-Cu	−110 ± 5	4.42 ± 0.05	4.36 ± 0.05	5.22
	Poly-Cu (oxidized)	+60 ± 5	4.59 ± 0.05	4.70 ± 0.05	5.22
	Ag (oxidized)	+470 ± 50	5.00 ± 0.05	5.28 ± 0.05	4.92
	70 nm Ag NPs (oxidized)	+190 ± 20	4.72 ± 0.05	4.9 ± 0.05	
	Au	+100 ± 10	4.63 ± 0.03	4.75 ± 0.05	
	70 nm Au NPs	+30 ± 5	4.56 ± 0.01	4.63 ± 0.05	
	30 nm Au NPs	−300 ± 30	4.23 ± 0.05	4.18 ± 0.05	
sp-Metals	Poly-Al	−430 ± 50	4.09 ± 0.03	3.92 ± 0.05	4.22
	70 nm Al NPs	−520 ± 50	4.00 ± 0.05	3.85 ± 0.05	
	70 nm Ga NPs	−150 ± 20	4.38 ± 0.05	4.30 ± 0.05	

phene due to the doping by the various metals and the corresponding WF of the metal-doped graphene. The theoretical WF values used by Giovanetti *et al.*[8] for metals, WF_M, are also reported for comparison to show the differences.

It is noteworthy that by plotting the shift of the graphene Fermi level, ΔE_F, due to metal doping as a function of the measured metal work function, WF_M, a linear trend is found as shown in Fig. 5, pointing out the following findings:

(i) for both n-type and p-type doping, the charge transfer is directly proportional to the measured metal, WF_M, indicating that, when the various effects of nanostructuring and oxidation on the WF are considered, the difference in the WF between the metal and graphene controls the charge transfer. From this it can be inferred that for the metals considered here, the intramaterial charge redistribution caused by the interface charge repulsion[55] is negligible, and charge transfer is the dominant factor.

(ii) sp-metals, both as thin film and NPs, primarily dope graphene n-type because of their lower WF.

(iii) Ag and Al are the metals that can give the largest p type-doping and n-type-doping respectively.

(iv) For all the metals investigated, including Au and Ag, the doping also depends on nanostructuring, since nanoparticles can have a WF lower than the corresponding bulk, and, as shown for Au, the doping can shift from p-type for thin films to n-type decreasing the size of Au nanoparticles. The n-doping of graphene by reducing the size of Au NPs found in this study is also consistent with n-doping of graphene by plasmon generated hot electrons in Au resonant nanoantennas reported by Fang *et al.*[57] revealed explicitly by electrical transport measurements.

(v) Unintentional oxidation of the metal can also dramatically alter the WF_M, as seen for Ag and Cu (see Fig. 6), also leading to a change from p-type to n-type doping or *vice versa*.

The theoretical WF of Al, reported to be 4.22 eV for (111) Al,[8] can further decrease to 3.75 eV by polycrystallinity and the presence of the native surface oxide[30,56] for Al NPs.[19] This change acts as a driving force for the transfer of electrons from Al to graphene, which is n-doped more efficiently.

The observed lower adhesion of graphene on oxidized Cu (as also corroborated by the XPS spectra in Fig. 6) results in an almost negligible charge transfer, which, however, is slightly p-type because of the higher work function of Cu-oxides, while it changes to n-type for graphene on clean Cu, consistent with previous reports.[58]

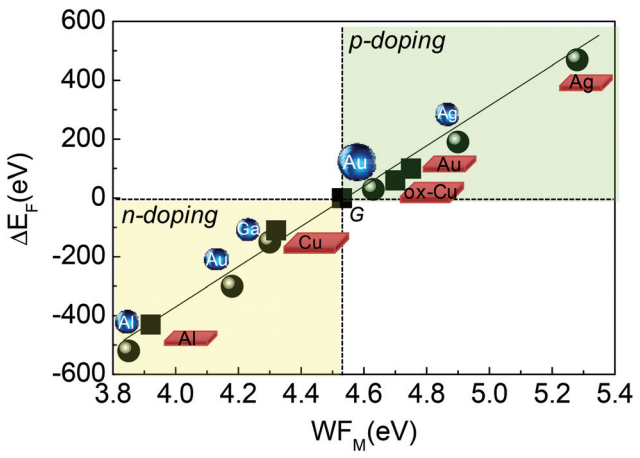

Fig. 5 Fermi level shifts, ΔE_F, of graphene samples doped by different metals, as both thin film (slab-symbol) and NPs (sphere-symbol) as a function of their work functions.

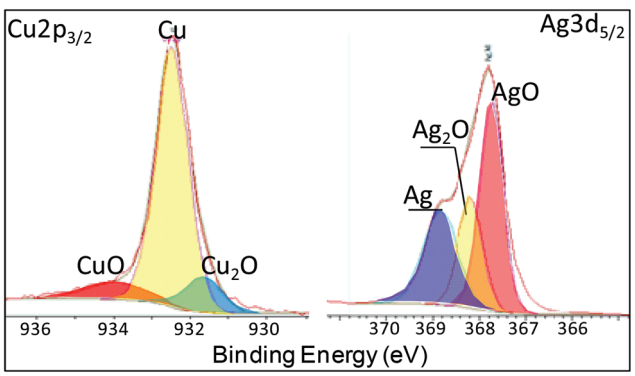

Fig. 6 XPS spectra of the Cu 2p3/2 and Ag 3d5/2 with fit components indicating the partial oxidation of Cu and Ag NPs underneath graphene.

Conversely, for Ag films and NPs, oxidation (see also XPS in Fig. 6) increases the WF from 4.3 to above 5 eV,[59] *e.g.*, WF values in the range from 4.78 ± 0.02 eV up to 5.53 ± 0.05 eV (for Ag NPs in the range 5–35 nm) have been measured and reported.[60,61] Those effects of oxidation and NP size provide an explanation for the experimentally observed strong p-doping of graphene by Ag.

It is noteworthy that Au, which is not affected by oxidation, provides an example of how the decrease of the WF with the decrease in Au NP size can invert the charge transfer and, consequently, the doping of graphene from the expected p-type to n-type with small Au NPs.

KPFM measurements have been corroborated by Raman spectroscopy, as shown in Fig. 7.

The Raman spectrum of the CVD graphene as-transferred on glass shows the G-band at ~1579 cm^{-1} and the single symmetric Lorentzian 2D band at ~2673 cm^{-1} with a peak intensity ratio $I_{2D}/I_G \sim 2.5$ typical of the graphene monolayer. The as-grown CVD graphene does not show any D peak related to defects. The D-peak is insignificant for many of the graphene-on-metal samples, especially for graphene transferred on metal films, as shown by the representative graphene on the Al film in Fig. 7b. A small D-peak is observed when graphene is transferred on some of the NP samples; in Fig. 7c we show the case of the graphene on the larger Au NPs (a similar situation was found for large Al NPs); for larger NPs we saw a higher probability to form ripples, wrinkles and defects because of the non-conformal covering of the NPs by the graphene, as also shown by AFM in Fig. 3.

It is well known that the Raman spectra of doped graphene samples show a blue-shift of the G-band, a shift of the 2D-band, which depends on the type of doping, and a variation of their relative intensity and of broadening as well.[62–64] Since the variation of the intensity of Raman peaks can be affected not only by the doping but, especially for graphene on NPs, by differentiated plasmonic enhancement,[18] we focus our attention on the shift of the G- and 2D-peak. Details of the shift of the Raman G- and 2D-peak as a function of the metal and of the used metal structure are shown in Fig. 7d and e. We measured a small blue-shift compared to that of Das *et al.*[62] and smaller specifically for those metals and NPs yielding n-doping. This can be explained considering that our transferred CVD graphene is intrinsically p-doped,[65] and this slight shift indicates, according to ref. 62, a reduction of the p-doping, moving to an n-doping. Fig. 7e provides details of the shift of the Raman 2D-band from which electronic interactions between the graphene and metal can be inferred. Indeed, the Raman data show a different slope for the p-type and n-type doping, being lower for the latter, consistent with the different trend reported for the 2D-shift from Das *et al.*[62] Furthermore, we observed that the 2D-shifts are larger than those of the G-peak, probably because of a mechanical strain[66,67] induced by the non-conformal covering of graphene to the metal, especially for graphene on NPs.

Because of the additional effect of strain on the shift of the Raman peak, we do not attempt a quantification of the doping

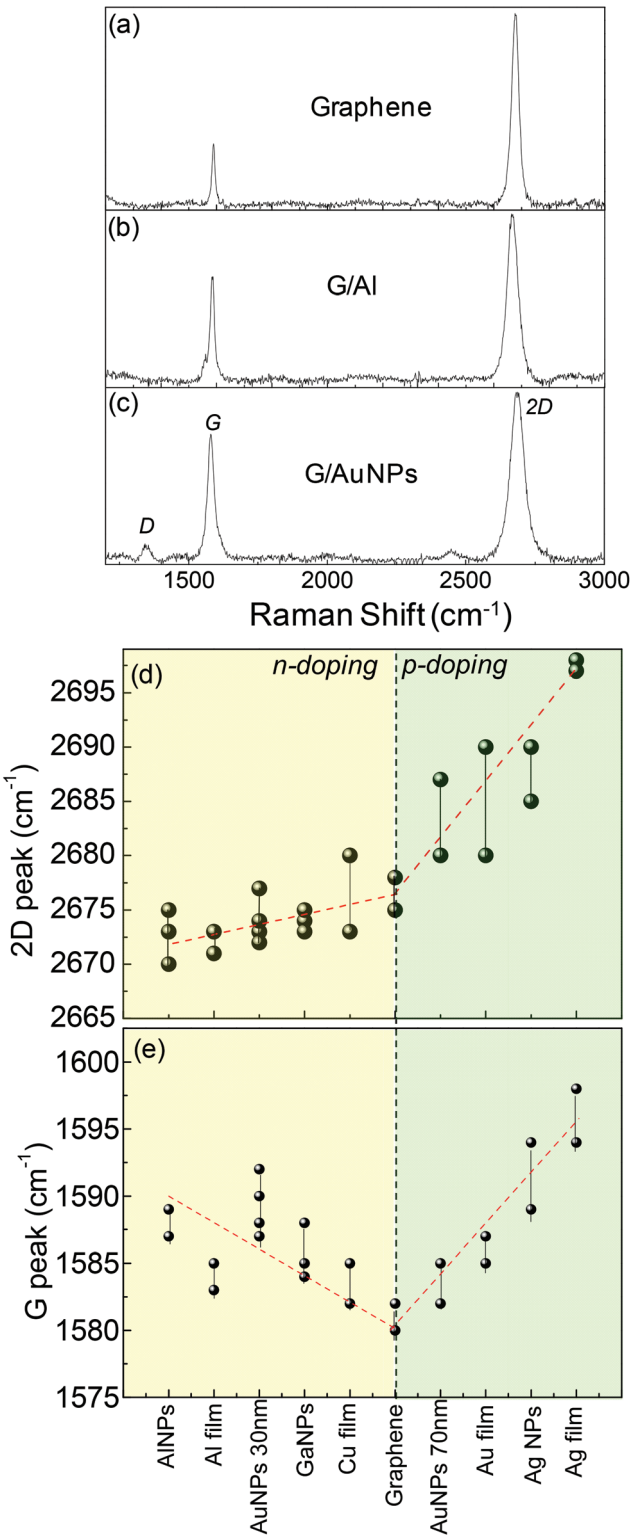

Fig. 7 Raman spectra of (a) as-grown graphene on glass, (b) graphene on the Al film and (c) graphene on 70 nm Au NPs. Shift of the (d) 2D-peak and of (e) G-peak for the various metal-doped graphene samples. In (d) and (e) the different points for the same metal refer to points measured on various produced samples for a reproducibility study.

concentration by Raman, but rather use it in a qualitative way to compare the Raman trends with data in Fig. 5 supporting the different doping of metals and NPs.

Additional independent information on the charge transfer is given by the ellipsometric analysis of the localized surface plasmon resonance (LSPR) of the metal NPs/graphene hybrids and of the plasma frequency, ω_p, which is proportional to the electron concentration, N, in the metal, being in the SI units $\omega_p{}^2 = \frac{Ne^2}{m_e\varepsilon_0}$ (where e is the electron charge, m_e is the effective mass of the electron, ε_0 is the permittivity of vacuum). Fig. 8 shows the variation of the ellipsometric spectra of the real part of the dielectric function, ε_1, with a focus on the Drude component at lower energy, for various metal films before and after graphene transfer ontop, as well as of the imaginary part of the pseudodielectric function, $\langle\varepsilon_2\rangle$, at the LSPR peak for the various metal NPs.

The spectra of the films have been modelled by a simple Drude model to derive the plasma frequency reported in the table at the top of Fig. 8. An increase of ω_p indicates an increase in the electron concentration in the metal (*e.g.* Au, Cu, Ag in the table in Fig. 8) as a consequence of charge transfer from graphene (p-doping), while a decrease in ω_p indicates a decrease in the electron concentration in the metal (*e.g.* Al in Fig. 8) as a consequence of charge transfer to graphene (n-doping).

Specifically, using the following values for the electron mass in the various metals[68] m_e (Al) = 0.97, m_e (Ag) = 0.99, m_e (Au) = 1.1, m_e (Cu) = 1.01, and the ω_p values in Fig. 8, we calculated the variation of electron density in the metal films upon graphene coupling as reported in the same table in Fig. 8. The reliability of the values determined for the various metals can be inferred comparing them with the reported[69] bulk free electron density of N(Al) = 2.1 × 10^{23} cm^{-3}, N(Au) = 5.9 × 10^{22} cm^{-3}, N(Cu) = 8.5 × 10^{22} cm^{-3} and N(Ag) = 5.86 × 10^{22} cm^{-3}. The determined lower values are consistent with the presence of grain boundaries in thin films of metals. Therefore, consistent with KPFM, the Al electron concentration decreases from 1.16 × 10^{23} cm^{-3} to 8.6 × 10^{22} cm^{-3} by transferring electrons to graphene; whereas, for example, the Au electron concentration increases from 4.77 × 10^{22} cm^{-3} to 5.75 × 10^{22} cm^{-3} by taking electrons from graphene that become p-doped. Interestingly, the variation of the electron concentration, *i.e.*, ΔN for the various metal films follows the same trend as KPFM data in Fig. 3, being ΔN for Al and Ag higher than that for Cu and Au.

On the other hand, the spectra of NPs/graphene are characterized by the LSPR peak, whose wavelength and amplitude depend on the plasma frequency of the metal and on the NP size.[70,71] Fig. 8 also highlights the different roles of sp-metals, since Al and Ga NPs are suitable for blue-UV plasmonics,[18] while Au NPs are active for visible-plasmonics.

When graphene is transferred on 70 nm Au NPs, the LSPR peak blue-shifts and narrows, while graphene on 30 nm Au NPs, Al NPs and Ga NPs causes a red-shift and broadening. Those opposite phenomena are indicative of an increase in electron density in the former case, which originates from an

	Al film	Au film	Cu film	Ag film
ω_p Metal (eV)	11.7±0.2	7.4±0.1	6.8±0.1	7.3±0.1
N (cm^{-3})	1.2·10^{23}	4.8·10^{22}	3.7·10^{22}	4.1·10^{22}
ω_p M with G (eV)	10.5±0.2	8.1±0.1	7.52±0.04	9.15±0.05
N (cm^{-3})	8.6·10^{22}	5.7·10^{22}	4.5·10^{22}	6.6·10^{22}

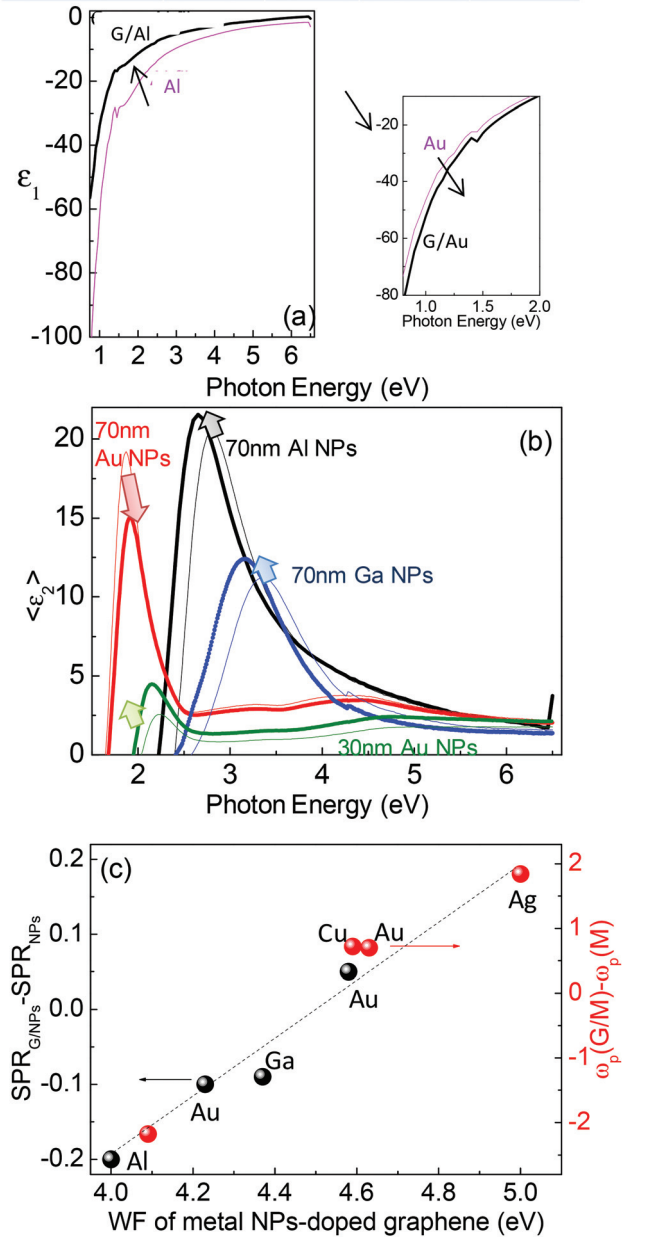

Fig. 8 Top: table of the plasma frequency, ω_p, for films of various metals (Au, Ag, Cu, Al) without and with graphene ontop, which also indicated the derived free electron concentration in the various metals. (a) Ellipsometric spectra of the real part of the imaginary part, ε_1, with focus on the Drude component for Al and Au films before and after transferring graphene ontop. (b) Variation of the ellipsometric spectra of the imaginary part of the pseudodielectric function, $\langle\varepsilon_2\rangle$, for various metal NPs before and after graphene transfer. (c) Summary of changes in the LSPR position of the metal NPs after graphene transfer, $SPR_{G/NPs}$–SPR_{NPs}, and of the plasma frequency, ω_pG/M–ω_pM upon graphene transfer as a function of the WF of metal-doped graphene.

electron transfer from the graphene to 70 nm Au NPs and, consequently, a p-doping of graphene, while the latter indicates a reduction of electron density in the smaller NPs, due to the electron transfer from the NPs to graphene and, consequently, an n-doping of graphene, consistent with the KPFM data.

Fig. 8c summarizes the shift of the LSPR position and the change in ω_p, induced by the graphene coupling. The blue shift of LSPR upon graphene transfer, *i.e.*, $SPR_{G/NPs}$–$SPR_{NPs} > 0$, indicates electron transfer from graphene to NPs, resulting in a p-doping of graphene. Conversely, the red-shift, *i.e.*, $SPR_{G/NPs}$–$SPR_{NPs} < 0$, supports the decrease of electron density in Ga and Al NPs as well as in small Au NPs, and, therefore, the n-doping of graphene. Therefore, KPFM and ellipsometry found a similar trend supporting the different roles of metals and nanoparticles in doping graphene.

4. Conclusions

In summary, we have measured the work function, WF, of metals and of graphene transferred on different metals, depending on nanostructuring and oxidation of the metals, using KPFM. We have considered metals representative of two main classes, *i.e.*, Ga and Al as sp-metals and Cu, Ag, Au as d-metals. We demonstrated that oxidation and nanostructuring of metals can significantly alter the WF of the metals. When the appropriate WF is considered for the metal, a linear relationship is found between the metal WF and the graphene doping. We have demonstrated that sp-metals efficiently dope graphene n-type. Although the case of indium (In) is not shown in this manuscript because of its faster oxidation of the In NPs, In WF < 4.1 also supports the n-doping of graphene. As for the d-metals, we found that decreasing the NP size and oxidation can affect significantly the metal WF and consequently the charge transfer direction. Specifically, the decrease of the Au and Ag NP size can reverse the charge transfer direction and change the graphene doping from p-type to n-type. Thus, the present work provides technology relevant guidance for tailoring doping of graphene and optimizing metal/graphene heterojunctions in devices.

Acknowledgements

The authors thank Mr A. Sacchetti for assistance in performing graphene synthesis and metal deposition experiments. We acknowledge the financial contribution of the European Commission under Grant Agreement 314578 "MEM4WIN". The author ML also acknowledges the CNR short mobility program "STM2014".

References

1 X. S. Li, W. W. Cai, J. H. An, S. Kim, J. Nah, D. X. Yang, R. Piner, A. Velamakanni, I. Jung, E. Tutuc, S. K. Banerjee, L. Colombo and R. S. Ruoff, *Science*, 2009, **324**, 1312–1314.
2 F. Xia, V. Perebeinos, Y.-M. Lin, Y. Wu and P. Avouris, *Nat. Nanotechnol.*, 2011, **6**, 179–184.
3 J. Zhu, Q. H. Liu and T. Linc, *Nanoscale*, 2013, **5**, 7785–7789.
4 C. Zhu and S. Dong, *Nanoscale*, 2013, **5**, 10765–10775.
5 C. Xu, X. Wang and J. Zhu, *J. Phys. Chem. C*, 2008, **112**, 19841–19845.
6 R. Muszynski, B. Seger and P. V. Kamat, *J. Phys. Chem. C*, 2008, **112**, 5263–5266.
7 N. Zhang, Y. Zhang and Y. J. Xu, *Nanoscale*, 2012, **4**, 5792–5813.
8 G. Giovannetti, P. A. Khomyakov, G. Brocks, V. M. Karpan, J. van den Brink and P. J. Kelly, *Phys. Rev. Lett.*, 2008, **101**, 026803.
9 C. Gong, G. Lee, B. Shan, E. M. Vogel, R. M. Wallace and K. Cho, *J. Appl. Phys.*, 2010, **108**, 123711.
10 P. A. Khomyakov, G. Giovannetti, P. C. Rusu, G. Brocks, L. van den Brink and P. J. Kelly, *Phys. Rev. B: Condens. Matter*, 2009, **79**, 195425.
11 M. Vanin, J. J. Mortensen, A. K. Kelkkanen, J. M. Garcia-Lastra, K. S. Thygesen and K. W. Jacobsen, *Phys. Rev. B: Condens. Matter*, 2010, **81**, 081408.
12 Y. Ren, S. Chen, W. Cai, Y. Zhu, C. Zhu and R. S. Ruoff, *Appl. Phys. Lett.*, 2010, **97**, 053107.
13 S. M. Song, J. K. Park, O. J. Sul and B. J. Cho, *Nano Lett.*, 2012, **12**, 3887–3892.
14 S. J. Park, H. Park, Y. Lee, Y. Yi and S. J. Kang, *J. Vac. Sci. Technol., B*, 2014, **32**, 011214.
15 Y. Wu, W. Jiang, Y. Ren, W. Cai, W. H. Lee, H. Li, R. D. Piner, C. W. Pope, Y. Hao, H. Ji, J. Kang and R. S. Ruoff, *Small*, 2012, **8**, 3129–3136.
16 A. Darhal, R. Addou, H. Coy-Diaz, J. Lallo and M. Batzill, *APL Mater.*, 2013, **1**, 042107.
17 D. Nobis, M. Potenz, D. Niesner and T. Fauster, *Phys. Rev. B: Condens. Matter*, 2013, **88**, 195435.
18 M. Losurdo, C. Yi, A. Suvorova, S. Rubanov, T.-H. Kim, M. M. Giangregorio, W. Jiao, I. Bergmair, G. Bruno and A. S. Brown, *ACS Nano*, 2014, **8**, 3031–3041.
19 X. Shi, G. Dong, M. Fang, F. Wang, H. Lin, W. C. Yen, K. S. Chan, Y. L. Chu and J. C. Ho, *J. Mater. Chem. C*, 2014, **2**, 5417–5421.
20 C. Gong, G. Lee, B. Shan, E. M. Vogel, R. M. Wallace and K. Cho, *J. Appl. Phys.*, 2010, **108**, 123711.
21 M. Hasegawa and K. Nishidate, *Phys. Rev. B: Condens. Matter*, 2011, **83**, 155435.
22 J. Lee, K. S. Novoselov and H. S. Shin, *ACS Nano*, 2011, **5**, 608–612.
23 K. S. Subrahmanyam, A. Manna, S. K. Pati and C. N. R. Rao, *Chem. Phys. Lett.*, 2010, **497**, 70–75.
24 M. S. Choi, S. H. Lee and W. J. Yoo, *J. Appl. Phys.*, 2011, **110**, 73305.
25 J. Park, W. H. Lee, S. Huh, S. H. Sim, S. B. Kim, K. Cho, B. H. Hong and K. S. Kim, *J. Phys. Chem. Lett.*, 2011, **2**, 841–845.
26 S. Yang, P. Zhou, L. Chen, Q. Sun, P. Wang, S. Ding, A. Jiang and D. W. Zhang, *J. Mater. Chem. C*, 2014, **2**, 8042.

27 M. M. Beerbom, B. Lagel, A. J. Cascio, B. V. Doran and R. Schlaf, *J. Electron Spectrosc. Relat. Phenom.*, 2006, **152**, 12–17.

28 D. Ziegler, P. Gava, J. Guttinger, F. Molitor, L. Wirtz, M. Lazzeri, A. M. Saitta, A. Stemmer, F. Mauri and C. Stampfer, *Phys. Rev. B: Condens. Matter*, 2011, **83**, 235434.

29 H. B. Michaelson, *J. Appl. Phys.*, 1977, **48**, 4729.

30 S. Brown, W. Osikowicz, Y. Wang and W. R. Salaneck, *Org. Electron.*, 2007, **8**, 14–20.

31 W. Osikowicz, M. P. de Jong, S. Braun, C. Tengstedt, M. Fahlman and W. R. Salaneck, *Appl. Phys. Lett.*, 2006, **88**, 193504.

32 S. Braun, W. R. Salaneck and M. Fahlman, *Adv. Mater.*, 2009, **21**, 1450–1472.

33 M. T. Greiner, L. Chai, M. G. Helander, W. M. Tang and Z. H. Lu, *Adv. Funct. Mater.*, 2012, **22**, 4557–4568.

34 A. Schmidt-ott, P. Schurtenberger and H. C. Siegmann, *Phys. Rev. Lett.*, 1980, **45**, 1284.

35 D. M. Wood, *Phys. Rev. Lett.*, 1981, **46**, 749.

36 M. Chelvayohan and C. H. B. Mee, *J. Phys. C: Solid State Phys.*, 1982, **15**, 2305–2312.

37 A. W. Dweydari and C. H. B. Mee, *Phys. Status Solidi A*, 1975, **27**, 223–230.

38 Y. Yang and S. W. Rhee, *Appl. Phys. Lett.*, 2007, **91**, 232907.

39 K. C. Kwon, K. S. Choi, B. J. Kim, J.-L. Lee and S. Y. Kim, *J. Phys. Chem. C*, 2012, **116**, 26586–26591.

40 X. Shen, H. Wanga and T. Yu, *Nanoscale*, 2013, **5**, 3352–3358.

41 M. Losurdo, M. Bergmair, G. Bruno, D. Cattelan, C. Cobet, A. de Martino, K. Fleischer, Z. Dohcevic-Mitrovic, N. Esser, M. Galliet, R. Gajic, D. Hemzal, K. Hingerl, J. Humlicek, R. Ossikovski, Z. V. Popovic and O. Saxl, *J. Nanopart. Res.*, 2009, **11**, 1521–1554.

42 M. Losurdo, M. M. Giangregorio, P. Capezzuto and G. Bruno, *Phys. Chem. Chem. Phys.*, 2011, **13**, 20836–20843.

43 G. Bruno, G. V. Bianco, M. M. Giangregorio, M. Losurdo and P. Capezzuto, *Phys. Chem. Chem. Phys.*, 2014, **16**, 13948–13955.

44 M. M. Giangregorio, M. Losurdo, G. V. Bianco, E. Dilonardo, P. Capezzuto and G. Bruno, *Mater. Sci. Eng., B*, 2013, **178**, 559–567.

45 W. Melitz, J. Shen, A. C. Kummel and S. Lee, *Surf. Sci. Rep.*, 2011, **66**, 1–27.

46 V. Palermo, M. Palma and P. Samorì, *Adv. Mater.*, 2006, **18**, 145–164.

47 C. Bustamante and D. Keller, *Phys. Today*, 1995, **48**, 32–38.

48 H. Takano, J. R. Kenseth, S. S. Wong, J. C. O'Brien and M. D. Porter, *Chem. Rev.*, 1999, **99**, 2845–2890.

49 H. Sugimura, Y. Ishida, K. Hayashi, O. Takai and N. Nakagiri, *Appl. Phys. Lett.*, 2002, **80**, 1459.

50 V. Panchal, R. Pearce, R. Yakimova, A. Tzalenchuk and O. Kazakova, *Sci. Rep.*, 2013, **3**, 2597.

51 T. Filleter, K. V. Emtsev, T. Seyller and R. Bennewitz, *Appl. Phys. Lett.*, 2008, **93**, 133117.

52 C. Oshima and A. Nagashima, *J. Phys.: Condens. Matter*, 1997, **9**, 1–20.

53 S. M. Choi, S. H. Jhi and Y. W. Son, *Phys. Rev. B: Condens. Matter*, 2010, **81**, 081407.

54 Y. Qi, J. R. Eskelsen, U. Mazur and K. W. Hipps, *Langmuir*, 2012, **28**, 3489–3493.

55 C. Gong, D. Hinojos, W. Wang, N. Nijem, B. Shan, R. M. Wallace, K. Cho and Y. J. Chabal, *ACS Nano*, 2012, **6**, 5381–5387.

56 T. Fort Jr. and R. L. Wells, *Surf. Sci.*, 1972, **32**, 543–553.

57 Z. Fang, Y. Wang, Z. Liu, A. Schlather, P. M. Ajayan, F. H. L. Koppens, P. Nordlander and N. J. Halas, *ACS Nano*, 2012, **6**, 10222–10228.

58 R. Blume, P. R. Kidambi, B. C. Bayer, R. S. Weatherup, Z. J. Wang, G. Weinberg, M. G. Willinger, M. Greiner, S. Hofmann, A. Knop-Gerickee and R. Schlo, *Nano Lett.*, 2015, **15**, 917–922.

59 J. B. Kim, C. S. Kim, Y. S. Kim and Y. L. Loo, *Appl. Phys. Lett.*, 2009, **95**, 183301.

60 M. Schnippering, M. Carrara, A. Foelske, R. Kotzc and D. J. Fermın, *Phys. Chem. Chem. Phys.*, 2007, **9**, 725–730.

61 A. Salehi-Khojin, H. R. M. Jhong, B. A. Rosen, W. Zhu, S. Ma, P. J. A. Kenis and R. I. Masel, *J. Phys. Chem. C*, 2013, **117**, 1627–1632.

62 A. Das, S. Pisana, B. Chakraborty, S. Pisacane, S. K. Saha, U. V. Waghmare, K. S. Novoselov, H. R. Krishnamurthy, A. K. Geim, A. C. Ferrari and A. K. Sood, *Nat. Nanotechnol.*, 2008, **3**, 210–215.

63 S. Piscanec, M. Lazzeri, F. Mauri, A. C. Ferrari and J. Robinson, *Phys. Rev. Lett.*, 2004, **93**, 185503.

64 M. Lazzeri and F. Mauri, *Phys. Rev. Lett.*, 2006, **97**, 266407.

65 G. V. Bianco, M. Losurdo, M. M. Giangregorio, P. Capezzuto and G. Bruno, *Phys. Chem. Chem. Phys.*, 2014, **16**, 3632–3639.

66 T. M. G. Mohiuddin, A. Lombardo, R. R. Nair, A. Bonetti, G. Savini, R. Jalil, N. Bonini, D. M. Basko, C. Galiotis, N. Marzari, K. S. Novoselov, A. K. Geim and A. C. Ferrari, *Phys. Rev. B: Condens. Matter*, 2009, **79**, 205433.

67 W. X. Wang, S. H. Liang, T. Yu, D. H. Li, Y. B. Li and X. F. Han, *J. Appl. Phys.*, 2011, **109**, 07C501.

68 S. O. Kasap, *Principles of Electronic Materials and Devices*, McGraw-Hill, 2nd edn, 2002, http://Materials.Usask.Ca.

69 H. Ibach l and H. Luth, in *Solid-State Physics-An Introduction to Principles of Materials Science*, Springer, 4th edn, 2009.

70 K. L. Kelly, E. Coronado, L. L. Zhao and G. C. Schatz, *J. Phys. Chem. B*, 2003, **107**, 668.

71 C. Noguez, *J. Phys. Chem. C*, 2007, **111**, 3806.